

CRITICALITY OF HOPF BIFURCATION IN PRECISION MOTION STAGE WITH PID AND TIME-DELAYED FEEDBACK CONTROLS

Sunit K. Gupta, Jiamin Wang, Oumar R. Barry*
 Department of Mechanical Engineering
 Virginia Tech, Blacksburg, Virginia 24061

ABSTRACT

The use of precision motion stages is very popular among advanced manufacturing and machining industries. However, the performance of these motion stages is usually undermined by friction-induced vibration. In this paper, we propose the use of time-delayed feedback control to minimize the undesirable effects of friction-induced vibrations. The use of time-delayed feedback control is well established in the literature; however, the use of time-delayed feedback control in PID controlled motion-stages has not been explored yet. Here, we consider a lumped parameter model of the PID controlled precision motion stage with a linear time-delayed state feedback control. The dynamical friction in the system is modeled using the LuGre model. Stability and nonlinear analysis of the system are carried out using analytical methods. The stability analysis reveals the existence of multiple stability lobes and codimension-2 Hopf points for a given choice of system parameters. Also, the nature of Hopf bifurcation is determined by using the method of multiple scales. We observe the existence of both subcritical and supercritical Hopf bifurcations in the system, depending on the choice of control parameters. This observation implies that the nonlinearity in the system could both be stabilizing or destabilizing in nature.

Keywords: Precision motion stage, LuGre model, method of multiple scales, subcritical and supercritical bifurcation.

INTRODUCTION

Due to the increase in demand for machine parts with micro-level pattern and nano-level surface finish in different applications, ultra-precision manufacturing machines with precision motion stages are being used intensively in advanced manufacturing and machining industries. In these industries, mechanical bearing based motion stages (MBMS) are more popular as compared to other motion stages due to their large motion range, high off-axis stiffness, and cost-effectiveness [1]. However, one of the phenomena plaguing the performance of PID controlled MBMS is the friction between the motion stage and the rigid supporting surface, which leads to friction-induced vibrations in the system. These friction-induced vibrations further cause long settling times, stick-slip phenomena, and large tracking errors [2, 3]. Therefore, to increase the performance of the motion stage, it is necessary to control/suppress the self-excited vibration. This step further requires a complete understanding of linear and nonlinear dynamics of the motion stage, which is the focus of current work.

To control these self-excited friction-induced vibrations, different methods have been developed and can be broadly classified into three categories: (1) application of advanced controllers [4, 5], (2) passive controllers [6, 7], and (3) time-delay feedback controllers [8–12]. However, the use of advanced and passive controllers in a complex system is limited due to algorithm complexity and practical range of design parameters, respectively [13–15]. In recent years, the use of time-delay feedback control has become prevalent to control vibration in complex systems [8, 9]. The use of time-delay feedback control,

* Address all correspondence to this author. Email: obarry@vt.edu

to suppress self-excited friction-induced vibration, was first explored by Das and Mallik [10]. Later on, Chatterjee [11] analyzed the control of different types of friction-induced instabilities using time-delay feedback control. Neubauer et al. [12] investigated analytically and experimentally the use of time-delay feedback control to quench stick-slip vibrations in an automotive disc brake.

We strongly emphasize that although the use of time-delay feedback control to suppress friction-induced vibration in the dynamical system is well-established in the literature, it has not been implemented to control friction-induced vibration in PID controlled motion stages. Therefore, this work is believed to be the first study to examine this problem, in which we use a linear time-delay feedback controller in a PID controlled motion stage to control the friction-induced vibrations. The dynamical friction in the system is realized through the LuGre model [16]. It has been observed that for a given set of control parameters in PID, the nature of bifurcation can be changed with the help of a time-delay feedback controller.

MATHEMATICAL MODEL OF MOTION STAGE

In this section, we briefly present the mathematical model of the motion stage employed for the current analysis. We model the precision motion stage as a lumped parameter, single degree of freedom model, which is in frictional contact with the rigid surface (as shown in Fig. 1). Therefore, if u_1 and u_2 are the feedback control forces corresponding to PID and time-delay controllers, respectively, m_t is the lumped mass of the motion stage, F_f is the frictional force between the motion stage and rigid surface, $r(t)$ is the setpoint/reference signal, and $x(t)$ is the motion of the stage, then the equation governing the motion of the stage is

$$m_t \ddot{X} = u_1 + u_2 - F_f, \quad (1)$$

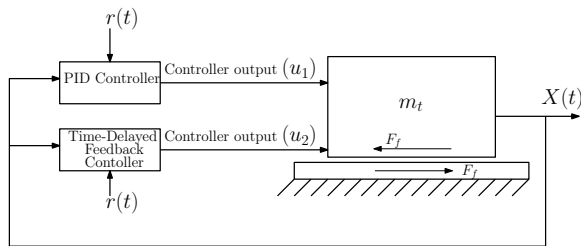


FIGURE 1: Schematic of PID controlled precision motion stage with time-delay feedback controller.

where controller forces u_1 and u_2 are

$$u_1 = -k_p^* \alpha - k_d^* \dot{\alpha} - k_i^* \int \alpha dt, \quad u_2 = K_0^* (\alpha(t - T^*) - \alpha(t)), \quad (2)$$

where k_p^* , k_d^* , and k_i^* represent the proportional, differential and integral gains, respectively, K_0^* represents the delay gain, T^* represents the time-delay and α represents the tracking error. Further, the tracking error α can be expressed in terms of $X(t)$ and

$r(t)$ as $\alpha = X(t) - r(t)$. Utilising the expressions for control forces, the equation of motion (Eq. 1) can be rewritten in terms of α as

$$m_t \ddot{\alpha} + k_d^* \dot{\alpha} + k_p^* \alpha + k_i^* \int \alpha dt = K_0^* (\alpha(t - T^*) - \alpha(t)) - F_f + m \ddot{r}. \quad (3)$$

In the current work, the frictional force F_f is determined by the LuGre friction model as it incorporates viscous friction, pre-motion friction (pre-sliding/pre-rolling), and hysteresis effects together [16]. If z represents the average bristle deflection (or the internal state variable), the friction force in the LuGre model can be defined as [16]:

$$F_f = \sigma_0^* z + \sigma_1^* \dot{z} + \sigma_2^* V_r, \quad (4)$$

where σ_0^* and σ_1^* are the contact stiffness the micro-damping of the bristle, respectively. σ_2^* is the macroscopic viscous friction between the contact surfaces, and $V_r = \dot{X} - \dot{\alpha} + \dot{r}$ is the relative velocity between the two moving surfaces. Also, the evolution of the average bristle deflection z with time is governed by [16, 17]:

$$\dot{z} = V_r - \frac{\sigma_0^* |V_r|}{g(V_r)} z = V_r \left(1 - \frac{\sigma_0^* \text{sgn}(V_r)}{g(V_r)} z \right), \quad (5)$$

where $g(V_r) > 0$ describes the Stribeck effect. For the analytical study of the system under study, we choose $g(V_r)$ as [17]:

$$g(V_r) = f_C^* + (f_S^* - f_C^*) e^{-\tilde{a}|V_r|}, \quad (6)$$

where f_C^* is the Coulomb friction, f_S^* is the static friction and \tilde{a} is the slope parameter. Note that Eqs. (3), (4), (5), and (6) together govern the complete dynamics of the system. Next, we define the following nondimensional scales and parameters to nondimensionalize the system of equation:

$$\begin{aligned} x &= \frac{\alpha}{X_0}, \quad \tilde{z} = \frac{z}{X_0}, \quad X_0 = \frac{g}{\omega_0^2}, \quad \omega_0 = \sqrt{\frac{k_p^*}{m_t}}, \quad \tau = \omega_0 t, \quad \zeta = \frac{k_d^*}{2m_t \omega_0}, \\ k_i &= \frac{k_i^*}{m \omega_0^3}, \quad T = \omega_0 T^*, \quad K_0 = \frac{K_0^*}{m \omega_0^2}, \quad v_r = \frac{V_r}{X_0 \omega_0}, \quad \sigma_0 = \frac{\sigma_0^*}{m_t \omega_0^2}, \\ \sigma_1 &= \frac{\sigma_1^*}{m_t \omega_0}, \quad \sigma_2 = \frac{\sigma_2^*}{m_t \omega_0}, \quad f_c = \frac{f_C^*}{m_t X_0 \omega_0^2}, \quad f_s = \frac{f_S^*}{m_t X_0 \omega_0^2}, \quad a = \tilde{a} \omega_0 X_0 \end{aligned}$$

Using the above-mentioned non-dimensional scales and parameters and assuming constant setpoint velocity ($\dot{r} = 0$), the governing equations of motion can be nondimensionalized and rewritten in state-space form as:

$$\dot{x}_1 = x_2, \quad (7a)$$

$$\dot{x}_2 = -2\zeta x_2 - x_1 - k_i x_3 + K_0 (x_1 (\tau - T) - x_1) - \left(\sigma_0 x_4 + \sigma_1 v_r \left(1 - \frac{\sigma_0 x_4}{g(v_r)} \text{sgn}(v_r) \right) + \sigma_2 v_r \right), \quad (7b)$$

$$\dot{x}_3 = x_1, \quad (7c)$$

$$\dot{x}_4 = v_r \left(1 - \frac{\sigma_0 x_4}{g(v_r)} \text{sgn}(v_r) \right), \quad (7d)$$

where $[x_1, x_2, x_3, x_4] = [x(\tau), \dot{x}(\tau), \int x d\tau, z(\tau)]$. Therefore, if v_{rv} represents the non-dimensional setpoint velocity, the non-dimensional relative velocity, v_r , will be $v_r = x_2 + v_{rv}$. For the

analytical study, we expand $\frac{1}{g(v_r)}$ in a Taylor series for smaller values of x_2 till third order and get

$$\frac{1}{g(v_{rv} + x_2)} = g_0 + g_1 x_2 + g_2 x_2^2 + g_3 x_2^3. \quad (8)$$

where g_i are the same as defined in [17]. Utilizing Eq. (7) and shifting the origin of the solution to the equilibrium state x_{is} as

$$x_i(t) = x_{is} + \varepsilon y_i(t), \quad \text{for } i = 1, 2, 3, 4 \quad (9)$$

where $y_i(t)$ s are shifted coordinates and $\varepsilon \ll 1$. Therefore, the equations of motion for pure slipping motion ($v_r > 0$) can be written in new coordinates as

$$\dot{y}_1 = y_2, \quad (10a)$$

$$\dot{y}_2 = K_0 y_1 (\tau - T) - (1 + K_0) y_1 - h_1 y_2 - k_i y_3 - h_2 y_4 + \varepsilon (h_0 \sigma_1 h_3 y_2^2 + \sigma_1 h_4 y_2 y_4) \quad (10b)$$

$$+ \varepsilon^2 (\sigma_1 h_5 y_2^3 + \sigma_0 \sigma_1 h_3 y_4 y_2^3) + \mathcal{O}(\varepsilon^3), \quad (10c)$$

$$\dot{y}_3 = y_1, \quad (10c)$$

$$\dot{y}_4 = -v_{rv} g_1 h_0 y_2 - v_{rv} \sigma_0 g_0 y_4 - \varepsilon (h_0 h_3 y_2^2 + h_4 y_2 y_4) - \varepsilon^2 (h_5 y_3^3 + \sigma_0 h_3 y_2^2 y_4) + \mathcal{O}(\varepsilon^3). \quad (10d)$$

where $h_0 = \frac{1}{g_0}$, $h_1 = \sigma_2 - h_0 \sigma_1 v_{rv} g_1 + 2\zeta$, $h_2 = \sigma_0 (1 - \sigma_1 v_{rv} g_0)$, $h_3 = (v_{rv} g_2 + g_1)$, $h_4 = \sigma_0 (g_0 + v_{rv} g_1)$, and $h_5 = h_0 (g_2 + v_{rv} g_3)$. Note that, we have already divided the expanded equation throughout by ε , to get the above perturbed delay differential equation (DDE). In the next section, we present the linear stability analysis to obtain the values of control parameters for the stable equilibrium.

LINEAR AND NONLINEAR ANALYSIS

In this section, the linear and nonlinear analyses of our system (using the method of multiple scales) are presented. We first start with the linear analysis as it provides the solution to the unperturbed linear equation, which will be used to form the solution for the perturbed nonlinear equation Eq. (10).

Linear Analysis

The linearized coupled system of the equation can be obtained by setting $\varepsilon = 0$ in Eq. (10) to obtain

$$\dot{y}_1 = y_2, \quad (11a)$$

$$\dot{y}_2 = K_0 y_1 (\tau - T) - (1 + K_0) y_1 - h_1 y_2 - k_i y_3 - h_2 y_4, \quad (11b)$$

$$\dot{y}_3 = y_1, \quad (11c)$$

$$\dot{y}_4 = -v_{rv} g_1 h_0 y_2 - v_{rv} \sigma_0 g_0 y_4. \quad (11d)$$

To get the characteristic equation, we substitute $y_i(\tau) = y_{i0} e^{\lambda \tau}$ (for $i = 1, 2, 3, 4$) in Eq. (11) and apply the solvability condition (the determinant of the coefficient matrix must vanish). This solvability condition further leads to the characteristic equation

which is transcendental in nature. The roots of these equation further determine the stability of the system. If all the roots lie in the left half-plane ($\Re(\lambda) < 0$) then the system is stable otherwise the system is unstable.

When the system loses its stability, a pair of complex conjugate roots crosses the imaginary axis ($\Re(\lambda) = 0$), and hence, Hopf bifurcation occurs. Therefore, in the occurrence of Hopf bifurcation, we let $\lambda = i\omega$ for $\omega > 0$ in the characteristic equation and accordingly, we separate real and imaginary parts as two algebraic equations. We solve these two equations for K_0 and T in terms of other system parameters and frequency as

$$K_{0,cr} = \frac{\Gamma_1}{\Gamma_2}, T_{cr} = \frac{1}{\omega} \left(2n\pi + \arctan \left\{ \frac{n_2}{d_2}, \frac{n_1}{d_1} \right\} \right) \quad \forall n = 0, 1, 2, \dots, \infty.$$

In the above expressions of $K_{0,cr}$ and T_{cr} , Γ_1 , Γ_2 , n_1 , n_2 , d_1 , and d_2 are the function of system parameters and frequency ω . For the sake of brevity these are not reported here. In the above expressions, n acts as a qualifier for the different stability boundaries and subscript 'cr' signifies values of control parameter at Hopf point. We emphasize here, that for a finite value of $K_{0,cr}$, the denominator of $K_{0,cr}$ should not be equal to zero, i.e., $\Gamma_2 \neq 0$. This constraint on Γ_2 further provides the lower limit on range of ω and can be obtained by setting $\Gamma_2 = 0$. Therefore, if ω_1 is the solution of $\Gamma_2 = 0$ then the effective range of ω , for the finite values of $K_{0,cr}$ and T_{cr} , becomes $(\omega_1, \omega_2]$ with $\omega_1 < \omega_2 < \infty$.

Since the solution of the linearized equation of the system (given by Eq. (11)) will be a periodic solution at the Hopf point, it can be written in terms of eigenvectors as

$$\mathbf{y}(\tau) = A_1 \mathbf{r}_1 e^{i\omega\tau} + A_2 \mathbf{r}_2 e^{-i\omega\tau} \quad (12)$$

where $\mathbf{y}(\tau) = [y_1(\tau), y_2(\tau), y_3(\tau), y_4(\tau)]^T$, A_1 and A_2 are the arbitrary complex conjugate constants, and \mathbf{r}_1 and \mathbf{r}_2 are the right eigenvectors of the characteristic matrix corresponding to eigenvalues $\lambda = i\omega$ and $\lambda = -i\omega$, respectively. Next, we present the nonlinear analysis of our system using the method of multiple scales.

Nonlinear Analysis Using The Method of Multiple Scales

The linear analysis of the system only helps us to determine the evolution of very small perturbation in stable and unstable regimes. However, the time evolution of these perturbations is truly determined by the nonlinearities present in the system. If all the perturbations decay with time and settle down to steady states in the linearly stable regime, then the steady states are globally stable. However, if small perturbations decay to steady states and large perturbations settle to limit cycles in the linearly stable regime, then the steady states lose global stability. Both of these dynamical characteristics of the system depend on the nature of nonlinearity, and hence, motivate us to carry out nonlinear analysis of the system.

For the nonlinear analysis, we use the method of multiple scales (MMS). With the introduction of multiple time scales (T_0, T_1, T_2) in the system, the solution of our perturbed nonlinear equation (Eq. (10)) can be assumed to be a series in powers of ε till $\mathcal{O}(\varepsilon^2)$ and written as

$$\mathbf{y}(\tau) = \mathbf{y}_0(T_0, T_1, T_2) + \varepsilon \mathbf{y}_1(T_0, T_1, T_2) + \varepsilon^2 \mathbf{y}_2(T_0, T_1, T_2) \quad (13)$$

Accordingly, the delayed value of the solution $\mathbf{y}(\tau - T)$ can be written as

$$\begin{aligned} \mathbf{y}(\tau - T) = & \mathbf{y}_0(T_0 - T, T_1 - \varepsilon T, T_2 - \varepsilon^2 T) \\ & + \varepsilon \mathbf{y}_1(T_0 - T, T_1 - \varepsilon T, T_2 - \varepsilon^2 T) \\ & + \varepsilon^2 \mathbf{y}_2(T_0 - T, T_1 - \varepsilon T, T_2 - \varepsilon^2 T) \end{aligned} \quad (14)$$

where $\mathbf{y}(\tau) = [y_1(\tau), y_2(\tau), y_3(\tau), y_4(\tau)]^T$. Now, to understand the effect of nonlinearity and hence, the nature of Hopf bifurcation, we perturb one of the control parameters close to the Hopf point such that the perturbed value lies in the unstable regime. For the current analysis, we choose time-delay T as the bifurcation parameter and accordingly, perturb T as

$$T = T_{cr} + \varepsilon^2 k_1, \quad (15)$$

where T_{cr} is the value of T at the Hopf point with $K_0 = K_{cr}$. On substituting Eqs. (14)-(15) in Eq. (10), expanding in Taylor series for smaller values of ε and equating the coefficients of different orders of ε to zero, we get coupled constant delay differential equations at different orders of ε . For the sake of brevity and space constrains these equations are not reported here and more details can be found in [18].

However, we emphasize here that order ε^0 equations are identical to the linearized unperturbed equations (Eq. (11)) with the control parameters at the Hopf point. Therefore, the solution for the equations at the order of ε^0 can be formulated as

$$\mathbf{y}_0(T_0, T_1, T_2) = A_1(T_1, T_2) \mathbf{r}_1 e^{i\omega T_0} + A_2(T_1, T_2) \mathbf{r}_2 e^{-i\omega T_0}. \quad (16)$$

Note that A_1 and A_2 instead of being complex conjugate constants are now complex conjugate function of slow time scales. On the substitution of the assumed form of the solution for \mathbf{y}_0 in the equations corresponding to ε^1 and following [17] we get the slow flow equations as

$$\frac{\partial R(T_2)}{\partial T_2} = p_{11} k_1 R + p_{12} R^3, \quad \frac{\partial \phi(T_2)}{\partial T_2} = p_{21} k_1 + p_{22} R^2, \quad (17)$$

where p_{11} , p_{12} , p_{21} , and p_{22} are functions of system and control parameters at the Hopf-point, and frequency. Equation (17) can also be used to determine the nature of Hopf-bifurcation. A detailed discussion on these slow flow equations and verification of our analytical approach with numerical simulation is presented in the next section.

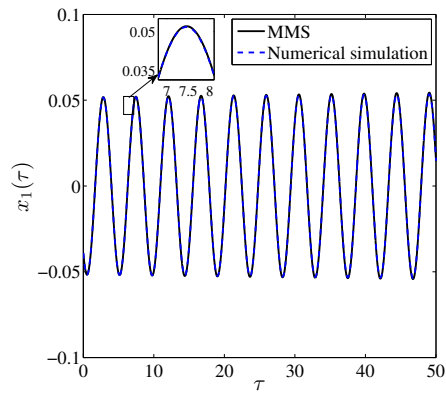
RESULTS AND DISCUSSION

In this section, we present results based on linear and nonlinear analysis of the system using MMS. For the analytical and

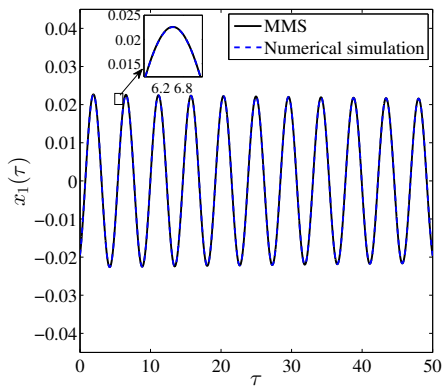
numerical analysis, we have used the following parameter values ([15]) $\omega_0 = 115.5$, $X_0 = 0.00073$, $\sigma_0 = 110$, $\sigma_1 = 1.37$, $\sigma_2 = 0.0823$, $f_s = 0.44$, $f_c = 0.35$, $a = 2.5$. Before proceeding further it is required to validate our analytical approach using MMS (slow flow equations). This validation can be achieved by comparing analytical results with numerical simulation using MATLAB routine 'dde23'. For this, we choose two different sets of parameters close to Hopf point at $K_0 = 0.5$ such that one point lies in the unstable regime ($T = 2.8716 > T_{cr} = 2.8715$) and another point remains in the stable regime ($T = 2.8714 < T_{cr} = 2.8715$). From Fig. 2, it can be easily observed that both approaches match very well with each other and hence, validate our analytical approach.

In the next step, we present the linear stability analysis of the system. The linear stability curves produced on the control parameter space of $T - K_0$ are shown in Fig. 3 for $\zeta = 0.2$ and different values of k_i . In the stability plot, the stable regions are marked by 'S' while the unstable regions are marked by 'U'. From Fig. 3, we can observe that multiple stability lobes exist corresponding to different values of $n = 0, 1, 2, \dots, \infty$. Also, from Fig. 3 we can easily observe that for a given value of ζ , there exists a critical value of k_i , say \bar{k}_i , below which multiple stability lobes (corresponding to different values of n) interact and the overall stability boundary will be the union of multiple stability lobes. However, we also emphasize here that for the values of $k_i < \bar{k}_i$, the stability lobe corresponding to $n = 0$ does not contribute in the primary stable region as it lies on the negative half-plane of T , which is not feasible for practical applications. Further, from Fig. 3b, we observe that for $k_i > \bar{k}_i$, there are no interactions between the stability lobes and also, the primary stability boundaries for this scenario is obtained by the stability lobe corresponding to $n = 0$ only (other stability lobes lies in the unstable regime). We notice that with further increase in k_i the overall stability decreases as evident from Fig. 3b. Now we present the criticality of Hopf bifurcation on the stability lobes using MMS. Note that the amplitude of limit cycles emerging from the Hopf point can be determined using the slow flow equations (Eq. (17)) and, eventually, the nature of bifurcation. If stable limit cycles near Hopf point exist in the unstable regime, then the bifurcation is supercritical in nature, which further implies that the system is globally stable and the nonlinearity in the system is stabilizing in nature. However, the existence of small-amplitude unstable limit cycles in the linearly stable regime leads to subcritical bifurcation, and eventually resulting in loss of global stability. To determine the nature of Hopf bifurcation and eventually the global stability of limit cycles close to Hopf point, we need to determine the steady-state amplitude of limit cycles. The amplitude of limit cycles close to Hopf point is determined by nontrivial fixed points of the slow-flow equations ($\dot{R} = 0$) and given by

$$R = \sqrt{\frac{-p_{11} k_1}{p_{12}}}. \quad \text{We emphasize here that quantity } p_{11} k_1 \text{ always}$$



(a)

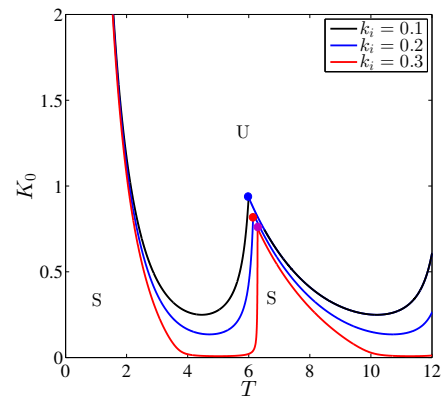


(b)

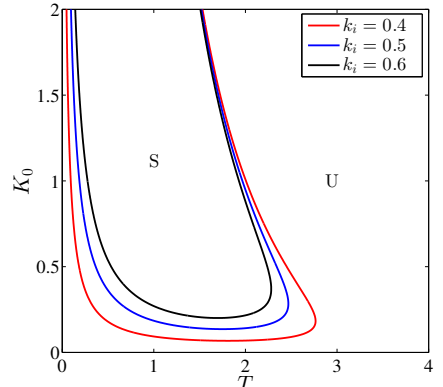
FIGURE 2: Comparison of time response of the system obtained from the MMS (solid line) and numerical simulation (dashed line) with (a) $T = 2.8716 > T_{cr} = 2.8715$, (b) $T = 2.8714 < T_{cr} = 2.8715$. Other parameters are $v_{rv} = 0.1$, $\zeta = 0.2$, $K_0 = 0.5$, $k_i = 0.1$

remains positive in the linear unstable regime and negative in the linear stable regime. Therefore, the nature of Hopf-bifurcation is governed by the sign of p_{12} only. If p_{12} is negative, then limit cycles will exist in linearly unstable regimes only and the Hopf bifurcation will be supercritical in nature. However, if p_{12} becomes positive, then the limit cycles will also exist in the linear stable regimes, and the Hopf-bifurcation will be subcritical in nature. Therefore, the set of control parameters on the stability boundary corresponding to transition point from subcritical to supercritical or vice-versa can be found by setting $p_{12} = 0$.

Using the information about the transition point, we present the stability boundaries with associated Hopf bifurcations for two different values of k_i , viz. $k_i = 0.1$ and $k_i = 0.4$ with $\zeta = 0.2$. On these curves, supercritical and subcritical bifurcation are marked with blue and red colors, respectively. From Fig. 4, we observe that for $k_i = 0.1$ due to the existence of multiple stability lobes we have a continuous transition from supercritical to subcritical bifurcation. However, for $k_i = 0.4$ there exists only one transition point on the primary stability and hence, the primary stability curve is divided into two branches of supercritical and subcritical



(a)

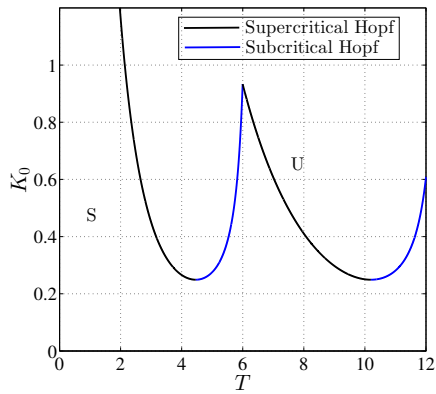


(b)

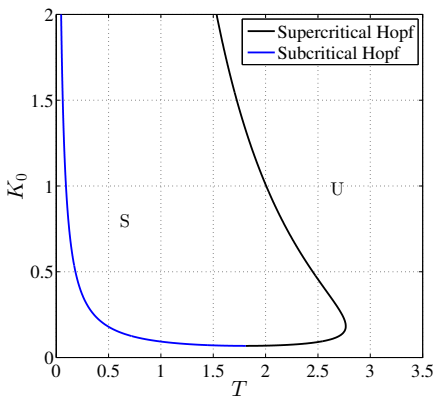
FIGURE 3: Stability curves in $(T - K_0)$ space for $\sigma_0 = 110$, $\sigma_1 = 1.37$, $\sigma_2 = 0.0823$, $\mu_s = 0.44$, $\mu_k = 0.35$, $v_{rv} = 0.1$, $\zeta = 0.2$, and $a = 2.5$ with different values of k_i corresponding to (a) multiple lobes, (b) single lobe.

bifurcation.

To further validate our analytical findings of subcritical and supercritical Hopf bifurcations, we also present the numerical bifurcation analysis. This step also helps us to get an understanding of the dynamics of the system away from the Hopf points. For the numerical bifurcation analysis, we have used MATLAB routine 'dde23' to solve our system of first-order delay differential equations (Eq. (7)). These bifurcation diagrams shows the extremum values for x_1 (corresponding to $x_2 = 0$). These bifurcation diagrams are plotted by fixing K_0 and varying T over a specified range in forward (increasing) and backward (decreasing) directions. The zoomed view of bifurcation diagrams at the Hopf point are shown in the inset of Fig. 5. From these bifurcation diagrams, we can observe that for $k_i = 0.1$ there is continuous transition in the nature of Hopf bifurcation from subcritical to supercritical or vice versa and only one transition for $k_i = 0.4$. We observe that both of the above-drawn observations for $k_i = 0.1$ and $k_i = 0.4$ are consistent with our analytical observations using MMS and further verifies our analytical findings. The overall dynamics of the system is very complex because of the appearance of period-2 and quasi-periodic solution, and its



(a)



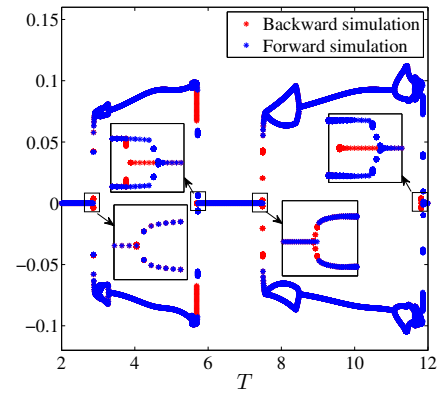
(b)

FIGURE 4: Stability boundary in the $T - K_0$ space depicting the supercritical and subcritical branches via black and blue dash lines, respectively, for (a) $k_i = 0.1$, (b) $k_i = 0.4$. Other parameters are $\nu_{rv} = 0.1$, $\zeta = 0.2$.

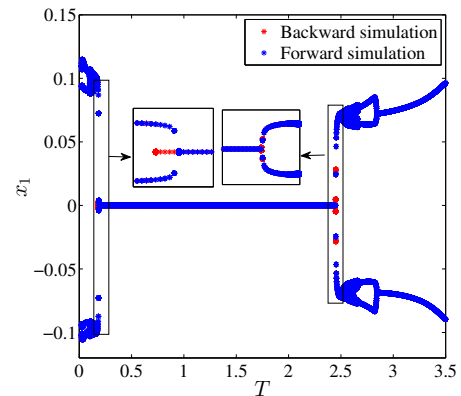
analysis has been left for future work.

CONCLUSION

This work examined the effect of time-delayed feedback controller on the global stability of a PID controlled precision motion stage. The effect of friction on the system was realized through the LuGre model. A parametric study on the linear stability of the system revealed that stability of the system is sensitive towards integral gain and stability of the system decreases as integral gain increases. Further, the existence of multiple stability lobes was observed for a range of values of integral gain. Nonlinear analysis using the method of multiple scales was performed on the system. We validated the analytical results via a comparison with numerical simulations. We observed a very good match between both approaches. Furthermore, the criticality of Hopf bifurcation was demonstrated on the stability curves. We observed a continuous or single transition of Hopf bifurcation from subcritical to supercritical or vice versa depending on



(a)



(b)

FIGURE 5: Numerical bifurcation diagram with T as bifurcation parameter for (a) $k_i = 0.1$, (b) $k_i = 0.4$. The other parameters are $\nu_{rv} = 0.1$, $\zeta = 0.2$, $K_0 = 0.5$.

the value of integral gain used in the analysis. This observation further suggested that nonlinearity in the system can be both stabilizing or destabilizing, in nature, depending on the system and control parameters. We further validated this criticality of bifurcation on the stability boundaries by performing numerical bifurcation analysis. Again, we observed a continuous or one transition from subcritical to supercritical bifurcation or vice versa, depending on the value of integral gain. These findings suggest that the performance of the time delayed controller for mitigating friction-induced vibration is significantly dependent on the integral gain in the system. We demonstrated that for given system parameters, there exists a range of integral gain at which large delay can also be utilized to suppress friction-induced vibration in the motion stage. We further observed the existence of codimension-2 Hopf point, period-2 and quasi-periodic solutions in the system. A detailed nonlinear analysis of the system has been left for future work.

ACKNOWLEDGEMENTS

This work is funded by National Science Foundation (NSF) CMMI #1855390: Towards a Fundamental Understanding of a Simple, Effective and Robust Approach for Mitigating Friction

in Nanopositioning Stages.

REFERENCES

- [1] Altintas, Y., Verl, A., Brecher, C., Uriarte, L., and Pritschow, G., 2011. "Machine tool feed drives". *CIRP annals*, **60**(2), pp. 779–796.
- [2] Marques, F., Flores, P., Claro, J. P., and Lankarani, H. M., 2016. "A survey and comparison of several friction force models for dynamic analysis of multibody mechanical systems". *Nonlinear Dynamics*, **86**(3), pp. 1407–1443.
- [3] Maeda, Y., and Iwasaki, M., 2012. "Rolling friction model-based analyses and compensation for slow settling response in precise positioning". *IEEE Transactions on Industrial Electronics*, **60**(12), pp. 5841–5853.
- [4] Dejima, S., Gao, W., Katakura, K., Kiyono, S., and Tomita, Y., 2005. "Dynamic modeling, controller design and experimental validation of a planar motion stage for precision positioning". *Precision engineering*, **29**(3), pp. 263–271.
- [5] Yao, J., Deng, W., and Jiao, Z., 2015. "Adaptive control of hydraulic actuators with lugre model-based friction compensation". *IEEE Transactions on Industrial Electronics*, **62**(10), pp. 6469–6477.
- [6] Dong, X., Liu, X., Yoon, D., and Okwudire, C. E., 2017. "Simple and robust feedforward compensation of quadrant glitches using a compliant joint". *CIRP Annals*, **66**(1), pp. 353–356.
- [7] Dong, X., and Okwudire, C. E., 2018. "An experimental investigation of the effects of the compliant joint method on feedback compensation of pre-sliding/pre-rolling friction". *Precision Engineering*, **54**, pp. 81–90.
- [8] Maccari, A., 2003. "Vibration control for the primary resonance of the van der pol oscillator by a time delay state feedback". *International Journal of Non-Linear Mechanics*, **38**(1), pp. 123–131.
- [9] Qian, C., and Tang, J., 2008. "A time delay control for a nonlinear dynamic beam under moving load". *Journal of Sound and Vibration*, **309**(1-2), pp. 1–8.
- [10] Das, J. K., and Mallik, A. K., 2006. "Control of friction driven oscillation by time-delayed state feedback". *Journal of Sound and Vibration*, **297**(3-5), pp. 578–594.
- [11] Chatterjee, S., 2007. "Time-delayed feedback control of friction-induced instability". *International Journal of Non-Linear Mechanics*, **42**(9), pp. 1127–1143.
- [12] Neubauer, M., Neuber, C.-C., and Popp, K., 2005. "Control of stick-slip vibrations". In *IUTAM Symposium on Vibration Control of Nonlinear Mechanisms and Structures*, Springer, pp. 223–232.
- [13] Lee, J. H., 2011. "Model predictive control: Review of the three decades of development". *International Journal of Control, Automation and Systems*, **9**(3), p. 415.
- [14] Dong, X., Okwudire, C., Wang, J., and Barry, O., 2019. "On the friction isolator for precision motion control and its dynamics". In *ASME 2019 International Design Engineering Technical Conferences and Computers and Information in Engineering Conference*, American Society of Mechanical Engineers Digital Collection.
- [15] Wang, J., Dong, X., Barry, O. R., and Okwudire, C. "Dynamical analysis of friction induced vibration in a precision motion stage with a friction isolator". *Submitted to Journal of Sound and Vibration*.
- [16] De Wit, C. C., Olsson, H., Astrom, K. J., and Lischinsky, P., 1995. "A new model for control of systems with friction". *IEEE Transactions on automatic control*, **40**(3), pp. 419–425.
- [17] Saha, A., and Wahi, P., 2014. "An analytical study of time-delayed control of friction-induced vibrations in a system with a dynamic friction model". *International Journal of Non-Linear Mechanics*, **63**, pp. 60–70.
- [18] Gupta, S. K., Wang, J., and Barry, O. R. "Nonlinear vibration analysis in precision motion stage with pid and time-delayed feedback controls". *Submitted to Nonlinear Dynamics*.